DESIGN OF THE BENDING AND QUADRUPOLE MAGNETS FOR THE MAIN RING OF THE JAPANESE 12 GEV PROTON ACCELERATOR

K. Endo and M. Kihara
National Laboratory for High Energy Physics
Oho-machi, Tsukuba-gun, Ibaraki, JAPAN

Abstract

The design features of the main ring magnet system of the Japanese 12 GeV proton accelerator are reported. Problems relating to the design of the dipole and quadrupole magnets are discussed, including choice of the core material and the results of field computation with magnetostatic programs.

Introduction

The proton accelerator is now being constructed at National Laboratory for High Energy Physics in Tsukuba district about 60 km northeast of Tokyo. The construction program started in 1971 and will end in 1975.

The design of the main ring magnet system was almost finished in 1971 and a contract was made in June 1972 for the fabrication of bending and quadrupole magnets between the Laboratory and Hitachi, Ltd. The first test magnet is scheduled to be delivered in November and after the test for several months the production will begin in April 1973. The accelerator enclosure will be completed by April 1973, and the first magnet will be installed in July. All magnets will be delivered by March 1974.

This proton accelerator is a so-called cascade type machine, and has a 500 MeV booster synchrotron as an injector, into which 20 MeV beams are injected from a linac. The preinjector is a 750 keV Cockcroft-Walton accelerator. This injection scheme has been investigated and reported elsewhere.[1]

The main ring magnet system consists of dipoles and quadrupoles. There are 56 quadrupoles, 28 focusing and 28 defocusing quadrupoles (designated as QF and QD, respectively), which are placed alternately in a regular fashion all along the ring.

The number of dipoles is 48 and they are regularly placed between QF and QD in the normal cell. In the long straight section two dipoles are dropped.

The design feature of the main ring magnets is the use of grain oriented decarburized steel as the core material. So far there is no large synchrotron magnet made of the oriented steel sheet. The usual oriented steel which contains about 3 % silicon exhibits excellent magnetic properties at low and intermediate fields, but it is not suitable for magnets which are energized up to high field such as 19 kG, since the saturation induction is rather low.

The oriented steel we plan to use for the main ring magnets is the decarburized steel containing 0.8 % silicon. The saturation induction for this oriented steel is higher by about 0.7 kG than the former. In this report, we will show that, using this oriented steel, high field correction lenses are almost unnecessary in our case.

As will be described in the following section, we have studied the magnet type, H or C for the dipole, and have chosen the C type magnet. In order to reduce sagitta, the dipole consists of two cores 1.61 m long. They are placed on the girder at an angle of 3.75 deg. and the common coils are wound around them.

Quadrupoles are not symmetric with respect to the 45 deg. axis of the quadrant since the required aperture is elliptical. The quadrupole with the thin return yoke on the sides has been adopted, which is convenient for the injection and the ejection of beams.

In this report we will describe the results of field computation and show the final design of the dipole and the quadrupole.

Parameters of the main ring

The parameters of the main ring are listed in Table 1.

The main ring is a separated function type synchrotron with the mean radius of 54 m. There are four superperiods in the ring, and each superperiod contains 7 unit cells. The cell structure is a symmetric FODO. The arrangement of magnets in the unit cell is shown in Fig.1.

Cell 'N' is the normal cell. The irregular cell designated as cell 'L' has the same structure as the normal cell except that the bending magnet after QF is omitted. The superperiod consists of 2 irregular cells and 5 normal cells, as shown in Fig.1. Since the focusing action of the bending magnet is so small compared with the quadrupole magnet, the betatron function is almost periodic with the period of the unit cell. The maximum and minimum betatron functions, β_{max} and β_{min}, are 20.5 m and 3.4 m, respectively. The momentum compaction factor is distorted by omitting bending magnets, and its maximum value is 3.8 m. The betatron frequency per turn is 7.25. The phase advance per cell is near 90 deg., which is very convenient for injection and ejection.

The long straight section is made of 2 irregular cells. Four long straight sections are used for the injection, the fast ejection to the bubble chamber, the slow ejection and the accelerating cavities. Two drift spaces, 5.46 m long each between QF and QD are available for special equipment such as the injection kicker, the ejection kicker,

Table 1 Parameters of the Main Ring

Maximum energy	12 GeV
Injection energy	500 MeV
Mean radius	54 m
Design Intensity	1×10^{13} ppp
Radius of curvature in bending magnets	24.6 m
Frequency of betatron oscillation per turn	7.25
Phase advance per cell	93.21°
Transition kinetic energy	5.4 GeV
Field strength in bending magnet	
at injection	1.48 kG
at final energy	17.5 kG
Field gradient in quadrupole magnet	
at injection	0.153 kG/cm
at final energy	1.80 kG/cm
Injection revolution frequency	0.670 MHz
Final revolution frequency	0.882 MHz
Harmonic number	9

the septum magnet and rf cavities.

The medium straight sections downstream of QF and QD are filled up with the installations such as beam position monitors, steering magnets, correcting quadrupole and sextupole magnets, and other special devices used for injection and ejection of the beams. The short straight sections after the bending magnets are used only for vacuum flanges.

The radius of the main ring is 9 times that of the booster. Therefore, 9 pulses from the booster are injected to fill up the ring during the injection flat porch which lasts more than 0.5 sec. It takes 0.45 sec to inject 9 pulses, since repetition frequency of the booster is 20 Hz.

The harmonic number of rf voltage in the main ring is selected to be 9 so that the injected beam can be captured in the stable region of the longitudinal phase space if the synchronization properly operates between the booster and the main ring. The rf frequency, then, ranges from 6.03 MHz to 7.94 MHz.

The useful aperture is 14 cm and 5.6 cm in the horizontal and vertical directions, respectively. Although the required aperture is different for QF and QD because of the different beam size, we adopted the same magnet for both QF and QD. As for the bending magnet, all magnets are the same.

The bending magnet is 3.22 m in the effective magnetic length. Since the magnetic rigidity of 12 GeV proton is 430 kG-m, the maximum guiding field is 17.5 kG. The field strength at injection is 1.48 kG, so that the remanence effect can be neglected.

The quadrupole magnet is 60 cm in the effective gradient length. The maximum gradient is 1.8 kG/cm.

The quadrupole magnets are energized by different power supply from the bending magnets. The field gradient must be regulated with respect to the field strength in the bending magnet in such a manner that the betatron frequency remains on the prescribed value in both transverse directions during the whole acceleration cycle. For this purpose, the specially designed power supply will be installed, by which the values of current in QF and QD can be changed independently within a certain amount.

The typical waveform for excitation of the main ring is shown in Table 2. The power supplies for the main ring magnets are so called static ones which means that the large pulsating load is directly supplied from the utility line. The detail of the power supply will be reported in the other paper in this conference.

Table 2 Typical waveform of excitation of the main ring

injection porch	0.5 - 0.75
rise time	0.75
flat top	0.5
fall time	0.5
total repetition time	2.25 - 2.5 sec

The physical layout of the main ring, including the injection transport line, the bubble chamber hall and the experimental hall, is shown in Fig.2. In addition to the fast and slow external proton beams, the main ring is equipped with the internal target station.

A typical cross section of the main ring enclosure is 4 m wide and 4.8 m high, as shown in Fig.3. The ring shaped building containing the magnet rests on concrete pillars driven into the sandstone layer about 10 m under ground. The concrete is made in eight separate sections, in order to prevent the concrete building from breaking when deformation of the ground happens. The sections are assembled with the 'expansion joints' by which the sections can move freely to each other in a certain amount.

The concrete building is covered by soil as shown in Fig.3 in order to shield radiation.

Material of core

Superiority of the grain oriented decarburized steel sheets as core material has been verified for the gradient magnet by one of authers.[2] Results obtained there are summarized below:

1. The field distribution inside the magnet gap is mainly determined by the magnetic property of the pole material in the direction perpendicular to the median plane. Thus, it is preferable to choose the rolling direction perpendicular to the median plane.
2. The field distribution can be estimated in good approximation by using the two-dimensional magnetostatic program, even in the case of oriented steel. Calculated and measured values coincide with accuracy better than 1 %.

3. As for the gradient magnet, use of tne oriented steel can raise the usable field range by 2 kG(i.e. from 15 kG to 17 kG).

The ordinary oriented silicon steel containing about 3 % silicon exhibits excellent magnetic properties in the rolling direction, especially at low and intermediate fields. The coercive force is very small (0.07 Oe) compared to the oriented decarburized steel (0.22 Oe). The B-H relation is shown in Fig.4 by the dotted curve. The oriented silicon steel is superior to the oriented decarburized steel up to 18.5 kG. However, because of a large amount of silicon content, the saturation induction is appreciably lowered.[3] Therefore, the ordinary oriented silicon steel is not suitable for the core material if the flux density in the return yoke rises beyond 19 kG.

On the contrary, the grain oriented decarburized steel contains less than 1 % silicon, so that the saturation induction may be higher by about 0.7 kG than oriented silicon steel. This is very important for the present case where average flux density reaches more than 19.5 kG.

Although the pure iron is the best with respect to the saturation limit of induction, it is so soft that workability is very bad. Thus, the small amount of silicon must be added in order to improve workability.

Along the line of development described in the previous paper, the production technique of the oriented decarburized steel has been further developed, and at present we can get the oriented steel sheet with higher permeability by 90 % than obtained before.

This is the unidirectionally oriented decarburized steel which contains about 0.8 % silicon. In Table 3 are shown the mechanical and magnetic properties of steel. In parentheses the characteristics of the oriented steel used as the core material of the gradient magnet model.[2] Comparing

Table 3 Mechanical and magnetic properties of low carbon, low silicon oriented steel

Tensile strength	> 23 kg/mm^2	(26.1)
Yield point	> 15 kg/mm^2	(18.3)
Elongation	> 25 %	(34.9)
Hardness	105	
Permeability at B=20 kG		
(L)	> 750 ± 15 %	(400 ± 28.3)
(C)	> 47 ± 5 %	(60 ± 3.3)
Flux density at H=40 Oe (B'_{40})		
(L)	> 20 kG ± 0.7 %	
Coercive force (B_m=18 kG)		
(L)	< 0.22 Oe ± 10 %	(0.244 ± 0.01)
(C)	< 0.47 Oe ± 10 %	(0.404 ± 0.01)

two kinds of oriented steel, roughly speaking, as magnetic properties in the rolling direction is improved, the properties in the perpendicular direction to rolling is deteriorated. The coercive force is also lowered as the grain orientation is enhanced.

In Fig.4 the B-H curves for both directions are shown. In this figure, for comparison, are shown the B-H relations for the ordinary oriented silicon steel.

The lamination thickness is 1 mm. Since the main ring is a slow cycling machine, the eddy current loss is negligibly small, despite the resistivity is lower than the silicon steel. Therefore, the thicker lamination is preferable in the view point of core fabrication. However, there is a practical limitation on thickness in the process of coating the insulation layer, and 1 mm is the practical limit.

The spread in field value from magnet to magnet must be less than 0.05 % (rms) from requirement that the closed orbit distortion should be reduced to a tolerable limit. At injection, the fluctuation in remanence and initial permeability is negligible as the injection field is rather high. Even if there would exist errors, the correction is easy. At high fields the closed orbit correction needs much more powerful magnets, so that it is desirable to make field error as small as possible.

As shown in Table 3, the fluctuation in the B-H relation is expected to be more or less 0.7 % at 20 kG. Thus, we are planning to shuffle steel sheet before punching in order to equalize the magnetic characteristics.

Bending magnet

Magnetic field computation

First of all, we compare the field distribution between the oriented steel and the ordinary non-oriented steel, and between C and H type magnets.

The field computation has been carried out by using the two-dimensional magnetostatic program SIBYL.[4] According to discussions in the previous paper, we have assumed that the magnetic property is isotropic instead of oriented, and the permeability is the one in the direction perpendicular to the median plane throughout the core.

In Figs. 5 and 6 are shown the examples of computational results for both types of magnet. Computation has been made at the field strength from 15 to 19 kG.

For comparison, we have decomposed the field distribution into the components of higher multipole by the least-squares method. The results are shown in Fig.7. For the H magnet, the quadrupole and the octupole components do not appear inherently as the magnet is symmetric with respect to the magnet centerline.

Interesting result is, as seen in Fig.7, that the sextupole component is almost the same for both types of magnet. This fact can be understood by considering that the sextupole component occurs mainly due to the saturation of the pole tip. This consideration is confirmed by the distribution of equipotential lines inside the pole. Consequently, it is expected that the sextupole component increases rapidly with increasing field strength, which is consistent with the computa-

tional result.

Another interesting result is that the quadrupole and the octupole components have maxima at a certain field strength and decrease at higher fields. These phenomena have been observed in the field measurement on the gradient magnet model.[5]

Difference in the field distribution between the oriented and the non-oriented steel is obvious. If we choose the non-oriented steel, we need a fairly large amount of correction lenses even at 17.5 kG.

In the following, we describe the final design of the pole shape.

The procedure to design the pole shape and to determine the pole width was divided into twosteps, such as

(a) to determine the pole profile which provides the required useful aperture at intermediate fields, and

(b) to design the pole shape at the extremities of the pole, which minimizes the saturation effect at high fields.

In the step (a), the position of the minimum gap was determined to be 10 cm apart from the centerline. The shim at the minimum gap is 0.3 mm, and there is a straight line of 1 cm in width which serves as a stacking guide in the core fabrication.

In Fig.8 the gradient distribution in the case of $\mu = \infty$ is shown.

In the step (b), the calculation was done using finite permeability values. In the investigation of the optimum pole shape at the extremities of the pole, it is relevant to choose, as a parameter, the ratio of roundness of the pole (a) and the half height of the minimum gap (g).[6]

Its optimum value, however, depends on the pole width and also on the magnetic property of the core material. In general, high field characteristics are improved by increasing the pole width, but increase in size of the magnet leads to the rise of the material and fabrication cost. So, we must decide the optimum value by compromising the field quality and the magnet size. In this design we finally determined the pole width to be 28 cm.

The optimum value of a/g for this pole width was around 1.5. The field distribution for the final pole shape is shown in Fig.8. This curve corresponds to the C magnet case and the field strength on the centerline is 17.5 kG.

Type of magnet

Three types of magnet have been investigated for the dipole magnet, i.e. the H magnet, the C magnet and the window-frame magnet.

The window-frame magnet is the best as for field quality and magnet size. However, there are following disadvantages with respect to fabrication process:

(1) The inner coil which is nearest to the aperture must be positioned precisely. The fabrication of the inner coil is difficult.

(2) The core must be split into upper and lower halves. Therefore, the fabrication processes such as punching and assembling double compared to the H or C magnet. According to initial inquiry, the fabrication cost, excluding the material cost, was almost twice as that for the H or C magnet. So we did not adopt the window-frame magnet.

As for comparison of the H and the C magnets, the H magnet has the following advantages over the C magnet;

(1) Weight of the magnet can be reduced by about 30 % if we use the H magnet instead of the C magnet.

(2) The field distribution is symmetric with respect to the magnet centerline in the case of the H magnet. This is essential when the homogeneity of field is desired up to higher fields.

(3) From the structural viewpoint the H magnet is much more rigid than the C magnet. Especially in core fabrication, the gap deformation during welding is the most troublesome problem in the case of the C magnet, while there is no problem in the H magnet.

On the other hand, the C magnet has the advantage that injection and ejection of beams are easy since the return yoke lies only on the inner side of the ring. This is specially the case for ejection from the short straight section, such as the secondary beam ejection using the internal target.

Another advantage of the C magnet is the accessibility to the vacuum chamber and the magnet gap.

In the present comparison, we have considered different kinds of magnet arrangement for the H and C magnets.[7] For the C magnet case, the unit magnet is made of two cores 1.6 m long each, which are placed on the girder at an angle of 3.75 deg. The common coils are wound around the cores. The maximum field strength is 17.5 kG. For the H magnet case, the coils are wound around each core and the length of the unit magnet is half of the C magnet. The maximum field strength for this case is 20 kG.

In Table 4, we summarize the weight of material, the power supply ratings and the construction cost. In this design current density of the exciting coil was chosen to be 10 A/mm^2. As seen from the table, the cost of magnet and power supply does not differ so largely that the choice of the magnet type should be made by the other factors.

Table 4 Comparison of the weight of material, the power supply ratings and construction cost between the C and H magnets

	C magnet	H magnet
Weight of iron (ton)	820	630
Weight of copper (ton)	33	40
Peak power (MW)	18.1	20.2
Average loss (MW)	2.63	3.23
Cost (M yen)		
Magnet	560	484
Power supply	543	612
Total	1103	1096

The most influential factor is the quantity of higher multipole components. In particular, as seen in Fig.7, the sextupole component is more than 10 times larger for the H magnet than for the C magnet. This is of course due to the higher field strength for the H magnet.

For the finally adopted shape of the C type bending magnet, the quadrupole, sextupole and octupole components are 0.0006 m^{-1}, 0.33 m^{-2}, and 0.63 m^{-3}, respectively.

Tolerance in systematic gradient error in the bending magnet is determined by the consideration that the operating point should not move across the nearest third resonance. The frequency shift due to this error is given in our case by the following;

$$\Delta\nu = 5 \times \frac{1}{B_0} \frac{\Delta B}{\Delta X}$$

Thus, for $\Delta\nu = 0.08$, the gradient error should be less than 0.015 m^{-1}. If we use the oriented steel, the correction is not necessary up to the maximum field. The octupole component is also small.

In conclusion, we have adopted the C magnet in preference to the H magnet for the following reasons;
(1) Fabrication cost including the power supply does not differ appreciably between the C and H magnet.
(2) Maximum field strength can be lowered for the C magnet, so that the field corrections at high fields are smaller for the C magnet than for the H magnet.
(3) The beam ejection is easier, since the return yoke lies on the inner side of the ring.
(4) Accessibility to the vacuum chamber and the magnet gap will be useful for maintenance of the accelerator.

Final design of magnet

The parameters of the bending magnet are shown in Table 5. In Fig. 9 is shown the cross section of the magnet. The core 1.61 m long is made by welding laminations to external bars under compression between thick end plates. Geometrical tolerance of the finished core is less than ± 0.05 mm. Lamination itself is punched in an accuracy better than ± 0.02 mm by the precise punching. The projection of the back of the core serves as a stacking guide during the stacking and welding process. After the core is welded, datum planes are machined to the upper bars.

Table 5 Parameters of the bending magnet

Total number of magnet	48	
Aperture H x V	140 x 56	mm^2
Length	3.22	m
Number of cores per magnet	2	
Unit core weight	7.1	ton
Unit coil weight	0.62	ton
Peak field	17.5	kG
Number of turns	32	
Total resistance	0.75	Ω
Total inductance	1.2	H
Peak current	3050	A

The coil is made of hollow copper conductor, which is insulated by glass mica type. It is impregnated under vacuum with epoxy resin. The yearly dose is expected to be more than 10^7 rad in the quiet area and 10^8 rad in the hottest part. The glass reinforced epoxy resin to be used can withstand more than 10^9 rad.

Quadrupole magnet

Magnetic field computation

The elliptical aperture is required for the quadrupole magnets. Quadrupoles with the symmetry axis at 45 deg. are desirable with respect to the higher multipole content. In this design, however, we have chosen the asymmetric pole, since it leads to reduction of the size of the magnet.

Another design feature is to make the return yoke on the sides as thin as possible, because the thin yoke is convenient for beam extraction.

The shape of the quadrupole has been determined by computing the gradient distribution with the two-dimensional magnetostatic program LINDA.[8] The position of the minimum gap and the shape of the shim were determined so that the required uniform gradient is obtained inside the elliptical aperture at the intermediate fields.

For the finally designed pole shape, the gradient distributions on both transverse axes, calculated under the assumption of $\mu = \infty$, are shown in Fig.10 by solid lines.

At the high field levels, the gradient distribution changes due to the saturation of the pole tip, especially on the horizontal axis. In Fig.10 are also shown the gradient distribution at the maximum field, when the ordinary non-oriented steel is used as the core material. On the vertical axis the field distribution does not deteriorate, since the field strength at the nose of the pole is not high, as seen in the B-map of Fig. 11. Around the minimum gap on the horizontal axis, the flux density in iron is above 19 kG, so that the saturation of the pole nose is serious.

The systematic gradient error in the quadrupole produces the betatron frequency shift. The relation between them is $\Delta\nu/\nu \simeq \Delta G/G$, so that the field deterioration is desired to be less than 0.5 %. Therefore, in the case of $\mu = \bar{\mu}$ shown in Fig.10, a small amount of correction is necessary.

In Fig.12 is shown the map of flux lines and equipotential lines inside the pole. As seen from the figure, it is apparent that the deterioration of field gradient on the horizontal axis is due to the saturation around the minimum gap, where the mmf drop is large compared with that in the pole tip on the vertical side. The figure attached to each equipotential line denotes the mmf drop measured in percent from the center of the yoke.

It should be noted, furthermore, that the flux are almost perpendicular to the horizontal

plane in the neighbourhood of the minimum gap on the horizontal axis. This fact suggests us that the field deterioration on the horizontal axis may be improved by using the oriented steel. The situation is just the same as the gradient magnet, if the rolling direction is chosen to be perpendicular to the horizontal plane. In this case the direction of flux lines becomes perpendicular to the rolling direction around the minimum gap on the vertical axis. However, this does not affect field gradient, since the permeability is still high.

In order to anticipate the improvement, we have investigated the effect of permeability on the field gradient. This calculation is based on the same assumption as in the dipole that the gradient distribution on each axis will be primarily determined by the magnetic property of iron in the flux direction, especially near the minimum gap in this case.

The calculated gradient distributions are shown in Fig.10 by dashed lines. The improvement in the field gradient on the horizontal axis is excellent if the permeability is high, while on the vertical axis the effect of decrease in permeability cannot be appreciated.

We can conclude, therefore, that the use of the oriented steel in the manner described above can improve the gradient distribution compared with the non-oriented case.

If the pole shape is symmetric with respect to the 45 deg. axis of the quadrant, the use of the oriented steel is not acceptable. Thus, the adoption of the asymmetric pole is effective for the improvement in field distribution in conjunction with use of the oriented steel.

Final design of magnet

The parameters of the quadrupole magnet are shown in Table 6. In Fig.13 is shown the cross section of the magnet. The core is made by welding. Upper and lower cores are assembled with the aid of guide keys of rectangular shape and the mate surfaces. Geometrical tolerance of the assembled core is more severe than the dipole. Thus,

Table 6 Parameters of the quadrupole magnet

Total number	56	
Radius of inscribed circle	50	mm
Length	60	cm
Unit core weight	1.5	ton
Unit coil weight	0.11	ton
Peak field gradient	1.80	kG/cm
Number of turns per pole	12	
Total resistance	0.56	Ω
Total inductance	0.25	H
Peak current	1570	A

lamination is punched in an accuracy of ± 0.015 mm. The lamination are stacked using as reference the pole and mate surfaces. The error of finished half core is within ± 0.03 mm to the specified value.

Conclusion

We summarize briefly the design feature of the main ring dipole and quadrupole.
(1) Oriented decarburized steel (0.8 % Si) is excellent for core material for both magnets.
(2) The C magnet is chosen for the dipole.
(3) The asymmetric pole is chosen for the quadrupole, which accommodates the required elliptical aperture.
(4) The return yoke on the sides for the quadrupole magnet is made as narrow as possible, since the magnetic deflection of ejection magnets can be reduced.

As for field computation, presently working magnetostatic programs can not treat the grain orientation of the steel sheet in the precise manner. We are considering the modification so as to treat the orientation effect.

Acknowledgement

Authors express their sincere thanks to Prof. T. Nishikawa for his continuous support and invaluable comments throughout this work. They are also indebted to Prof. T. Doke for his valuable discussions.

References

1. T. Kamei et al., Proc. 8th Int. Conf. on High Energy Accelerators, CERN, 1971, M.H. Blewett, Editor, p.120. As for booster magnet, a paper will be submitted to this conference.

2. T. Doke et al., Nucl. Inst. Meth. 83, 300 (1970).

3. H. Brechna, Proc. 2nd Int. Conf. on Magnet Technology, Oxford, 1967, p. 305.

4. J.H. Dorst, Proc. 1st Int. Conf. on Magnet Technology, Stanford, 1965, H. Brechna and H.S. Gordon, Editor, p.182.

5. T. Hirose and H. Sasaki, "High-Field Measurement of Model Magnet, Mark I, II, III and IV for Proton Synchrotron, SJC-A-70-1 (1970), Working Group for Construction of Proton Synchrotron, Institute for Nuclear Study, Univ. of Tokyo.

6. M. Kihara and T. Doke, Nucl. Inst. Meth. 66, 45 (1968).

7. K. Endo and M. Kihara, KEK-report, to be published, National Laboratory for High Energy Physics.

8. J.S. Colonias and J.H. Dorst, Proc. 1st Int. Conf. on Magnet Technology, Stanford, 1965, H. Brechna and H.S. Gordon, Editor, p.188.

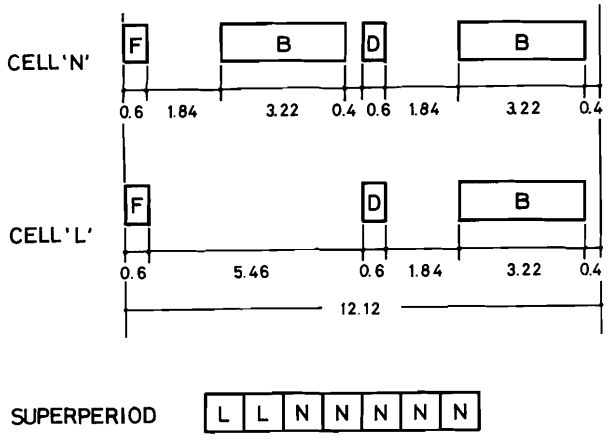

Fig. 1. Cell structure.

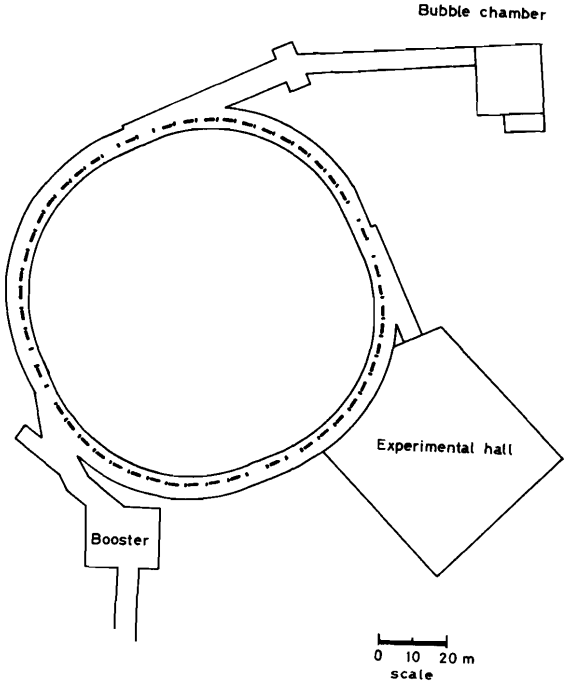

Fig. 2. Layout of the main ring.

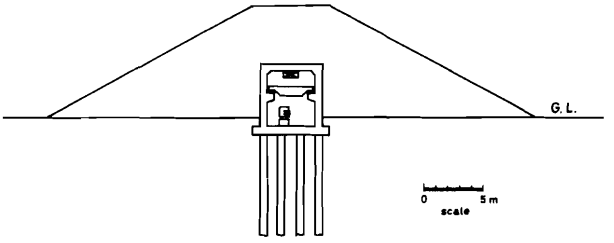

Fig. 3. Typical cross section of the enclosure.

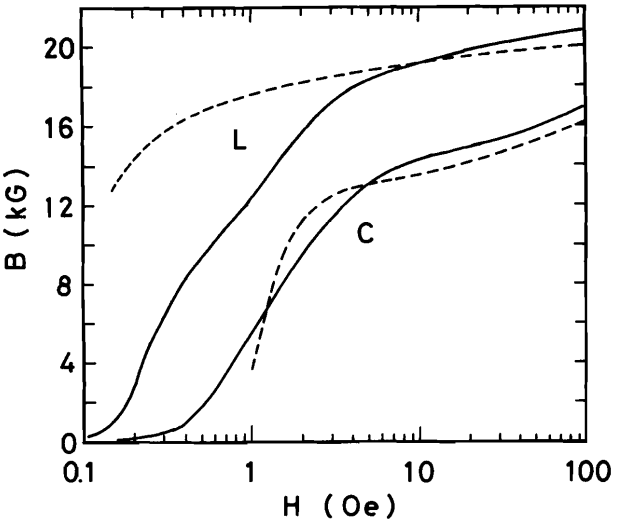

Fig. 4. B-H curves of oriented decarburized steel (solid line) and oriented silicon steel (dashed line) in the roll direction (refered to the 'L' direction) and the direction perpendicular to the rolling (refered to the 'C' direction).

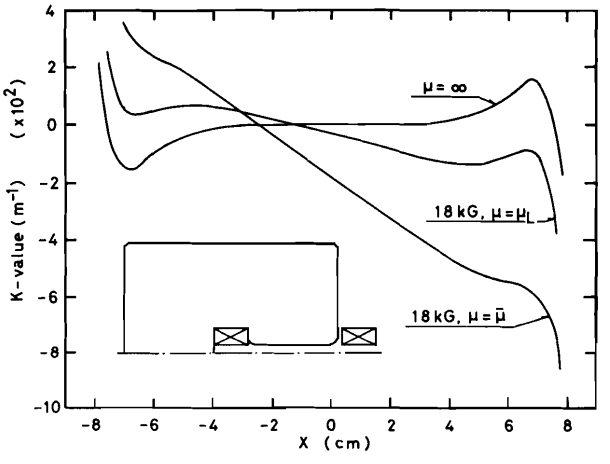

Fig. 5. Calculated gradient distributions for the C magnet. The field strength is 18 kG. The K value is defined as $K = (1/B_0)(\partial B/\partial x)$. μ_L and $\bar{\mu}$ correspond to oriented steel and non-oriented steel, respectively.

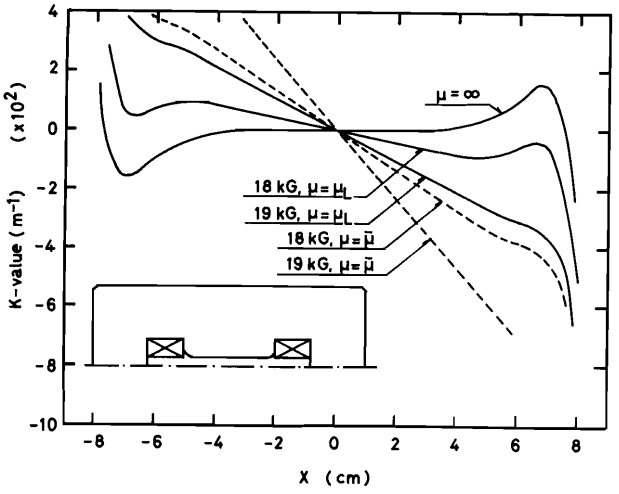

Fig. 6. Calculated gradient distributions for the H magnet. The field strength is 18 and 19 kG.

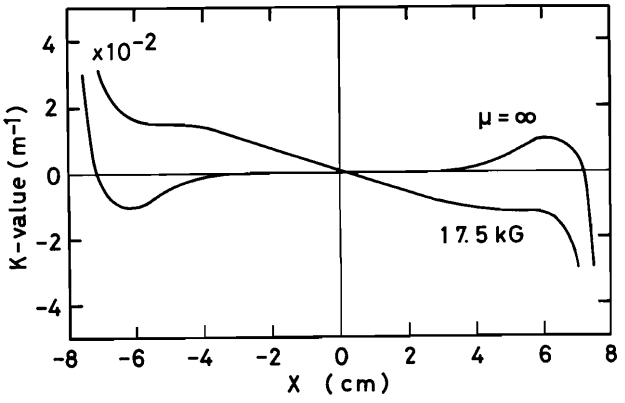

Fig. 8. Gradient distributions for the finally adopted C-type magnet at the intermediate and maximum fields.

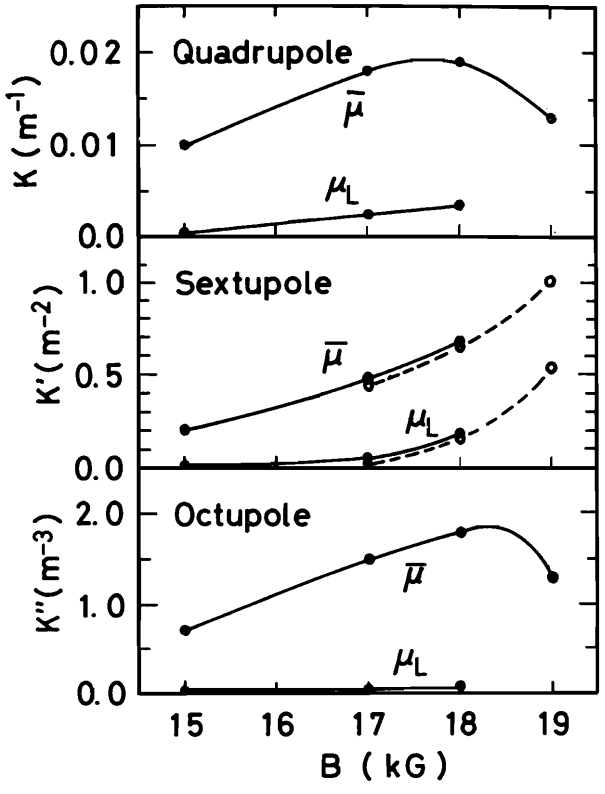

Fig. 7. Higher multipole components of the field gradient for the C magnet (solid line) and the H magnet (dashed line).

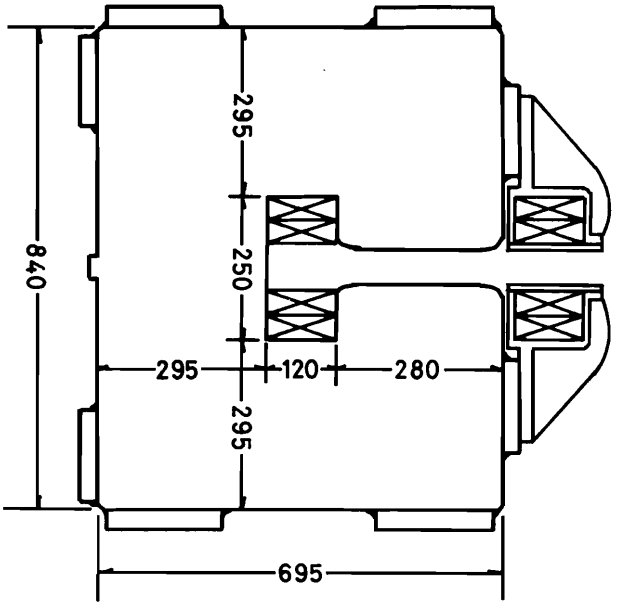

Fig. 9. Cross section of the bending magnet.

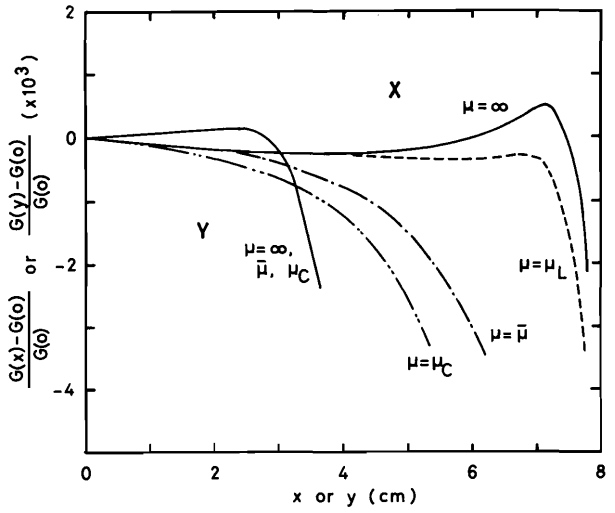

Fig. 10. Gradient distributions for the quadrupole on both x and y axis. μ_L and μ_C correspond to permeability of the L and C directions. $\bar{\mu}$ corresponds to non-oriented steel. G(x) and G(y) denote the field gradient on the x and y axes. G(0) is the gradient at the quadrupole center.

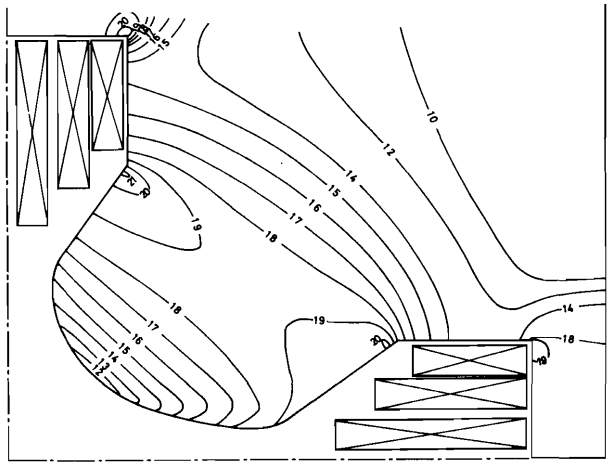

Fig. 11. B-map in the pole. The field gradient is 1.8 kG/cm which corresponds to the maximum energy. Unit is in kG.

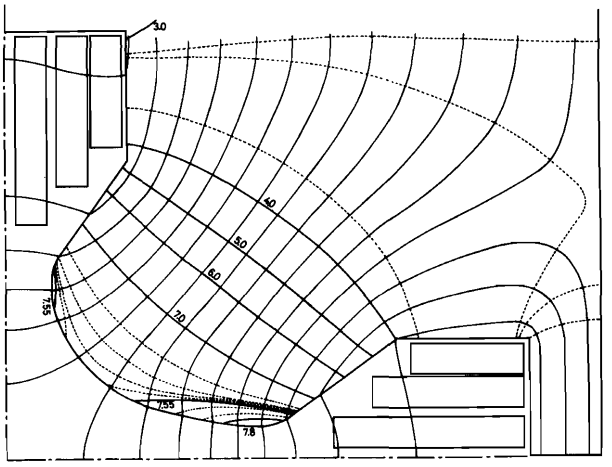

Fig. 12. Flux lines and equipotential lines inside the pole. Figures assigned to equipotential lines are the percentage drop of mmf.

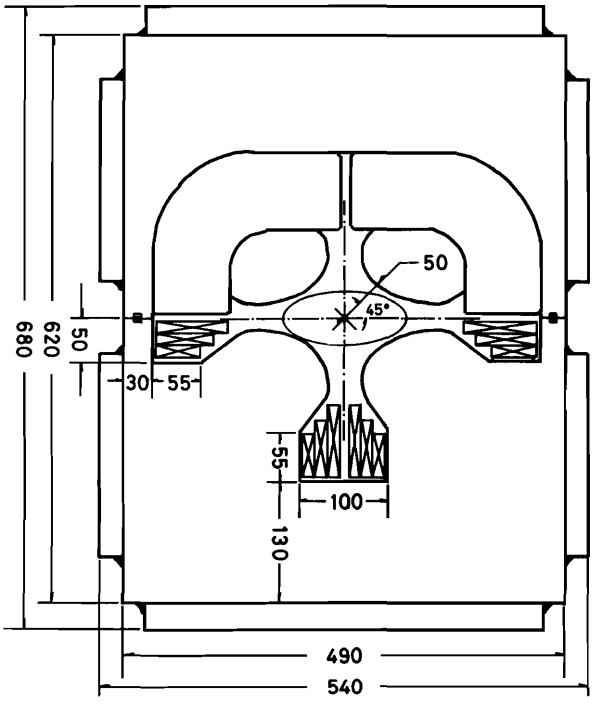

Fig. 13. Cross section of the quadrupole magnet.